J Electroceram (2012) 28:268–274
DOI 10.1007/s10832-012-9727-2

Structural and electrical studies of $Ba_5LaTi_3V_7O_{30}$ compound

Kiran Kathayat · A. Panigrahi · A. Pandey · S. Kar

Received: 16 December 2011 / Accepted: 3 April 2012 / Published online: 26 April 2012

Abstract The ferroelectric ceramic $Ba_5LaTi_3V_7O_{30}$ has been synthesized by solid-state reaction technique. Preliminary X-ray structural analysis confirmed a single-phase formation (orthorhombic crystal system) of the compound. Surface morphology of the compound was studied by scanning electron microscopy (SEM). Detailed studies of electrical properties (i.e., dielectric constant, loss tangent, ac and dc conductivity) as a function of temperature (RT - 773 K) at four different frequencies, 1 kHz, 10 kHz, 100 kHz and 1 MHz show ferroelectric—paraelectric phase transition of the compound. The impedance spectra show two distinctly separated regions in wide temperature range corresponding to grain boundary and grain interior contributions. The activation energy has been evaluated from ac conductivity and dc conductivity following Arrhenius equation is 0.15 eV at 1 MHz and 0.28 eV, respectively. The temperature dependence of electrical conductivity shows that the conductivity increases with increase in temperature suggesting that the compounds have a negative temperature coefficient of resistance (NTCR) behaviour. The conductivity pattern shows that it is strongly frequency dependent and obeys Jonscher's power relation.

Keywords Solid-state reaction · Dielectric constant · Loss tangent · Arrhenius equation · AC and DC conductivity

K. Kathayat (✉) · S. Kar
Department of Physics, North Orissa University,
Baripada 757003, Orissa, India
e-mail: kathayatkiran@yahoo.in

K. Kathayat
e-mail: kathayatkiran@gmail.com

A. Panigrahi
Department of Physics, D.N. College,
Itanagar 791111, Arunachal Pradesh, India

A. Pandey
Department of Physics, North Eastern Regional Institute of Science & Technology,
Nirjuli 791109, Arunachal Pradesh, India

1 Introduction

The study of compounds having TB [1–4] structure provides flexibility of cations substitutions at various sites. The tungsten bronze structure is complex with a general formula $[(A_1)_2(A_2)_4(C)_4]$ $[(B_1)_2(B_2)_8]O_{30}$ [5], where the A site can have di or trivalent cations and the B can be tri or pentavalent cations. This structure has BO_6 octahedrons sharing the corner forming three interstitial sites. Generally, the smallest interstice C site is empty, so a general formula of TB structure can be written as $A_6B_{10}O_{30}$ for filled (TB) structure. Thus, it provides a scope of wide variety of cations substitution [6] which have been widely used for a variety of scientific and industrial applications such as capacitor, sensors, electro-optic devices [7, 8] etc. TB type ferroelectrics, niobates are prominent because of electro-optic uses. Examples of this type of ferroelectrics are $PbNb_2O_6$, (Pb-Ba) Nb_2O_6, (Ba-Sr)Nb_2O_6, BNN (barium-sodium niobate) [9].

New materials with TB structure [10–13] having interesting properties have been discovered. Among them are rare-earth doped niobate-titanate; $Ba_5RTi_3Nb_7O_{30}$ (R=Eu, Gd) [14] which show diffuse phase transition [15] with T_c variation with rare-earth. But the problem with this compound is that it can only be sintered at high temperature (~1473 K) in order to form required phase with desired properties. In recent studies, it has been shown that the replacement of niobium with vanadium in $Ba_5RTi_3V_7O_{30}$ (R=Ho) brings down sintering temperature considerably

(~1073 K) [16]. Although the structural and dielectric properties of $Ba_5HoTi_3V_7O_{30}$ [16] has examined; in this paper we reporting the structural, microstructural, dielectric and electrical conductivity of $Ba_5LaTi_3V_7O_{30}$ ceramic synthesized by solid state reaction.

2 Experimental

The $Ba_5LaTi_3V_7O_{30}$ (BLTV) electroceramic has been prepared by the high temperature solid-state reaction method using as precursor salts $BaCO_3$ (Loba chemie, 99 %), La_2O_3 (Merck, 99.5 %+) , TiO_2 (Loba chemie, 99.5 %) and V_2O_5 (Loba chemie, 99 %). The physical mixtures of above ingredients were mixed and ground thoroughly in agate in methanol environment to maintain proper stoichiometry and homogeneity. The powder was then calcined in alumina crucible at 1023 K for 12 h. Time and temperature for calcination was selected after optimizing these parameters. The calcined powder was thoroughly mixed with PVB as binder. The process of grinding and calcinations was repeated until the formation of compounds was confirmed. The calcined powder were pressed into cylindrical pellets of diameter 12–13 mm and thickness 1–2 mm with polyvinyl butyral (PVB) as the binder, using a hydraulic press at a pressure of ~7 tons. The pellets were then sintered in an air atmosphere at 1073 K for 12 h, and then polished with fine emery paper to make their faces flat and parallel. The pellets were finally coated with conductive silver paint and dried at 423 K for 2 h before carrying out impedance measurements. X-ray diffraction (XRD) studies of the materials were carried out at room temperature in the Bragg angle range 20°–80° by an X-ray diffractometer. Surface morphology of the compound was studied by scanning electron microscopy (SEM). The impedance measurements were carried out at an input signal level of 300 mV in the temperature range of RT-773 K using a computer-controlled impedance analyzer (HIOKI LCR Hi TESTER, Model: 3532–50) in the frequency range of 42Hz–5 MHz along with a laboratory made sample holder and a heating arrangement.

3 Results and discussion

3.1 Structural study

The room temperature XRD pattern (Fig. 1) of the calcined powder shows the formation of single-phase compound. The reflection peaks of the pattern were indexed in tetragonal or orthorhombic crystal system using computer software "POWDMULT" [17] since TB compounds have tetragonal or orthorhombic crystal structure. An orthorhombic unit cell was selected on the basis of the best agreement between observed and calculated interplanar spacing d (i.e., $\Sigma\Delta d=\Sigma(d_{obs}—d_{cal})$=minimum). The lattice parameters of the selected unit cell are: a=7.1796 Å, b=4.0513 Å and c=26.8541 Å. The unit cell parameters are consistent, and are in good agreement with those reported earlier for TB structural family.

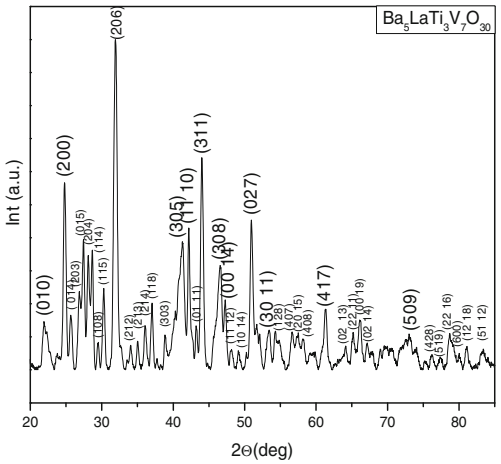

Fig. 1 XRD pattern of $Ba_5LaTi_3V_7O_{30}$

3.2 Microstructural study

Figure 2 shows SEM micrograph of the sintered pellet at room temperature. It is found that the grains are of platelet like morphology and size are non-uniform and densely distributed throughout the sample. A certain degree of porosity persists which may be due to the low sintering temperature. The average grain size of the compound was found as ~3 μm. The shape, size and distribution of grains in the microstructure suggest that the sample has polycrystalline nature. Similar microstructures are observed with that of some other materials of this family [16].

3.3 Dielectric properties

The temperature dependent (a) dielectric constant (ε_r) and (b) loss tangent (tanδ) are shown in Fig. 3 at selected frequencies (1 kHz, 10 kHz, 100 kHz and 1 MHz).

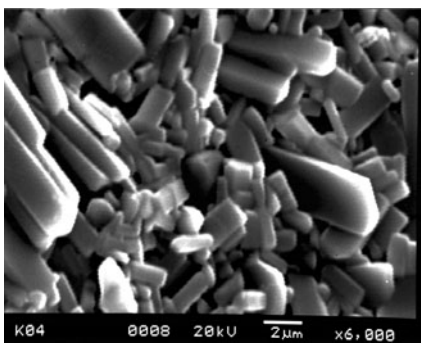

Fig. 2 SEM micrograph of $Ba_5LaTi_3V_7O_{30}$

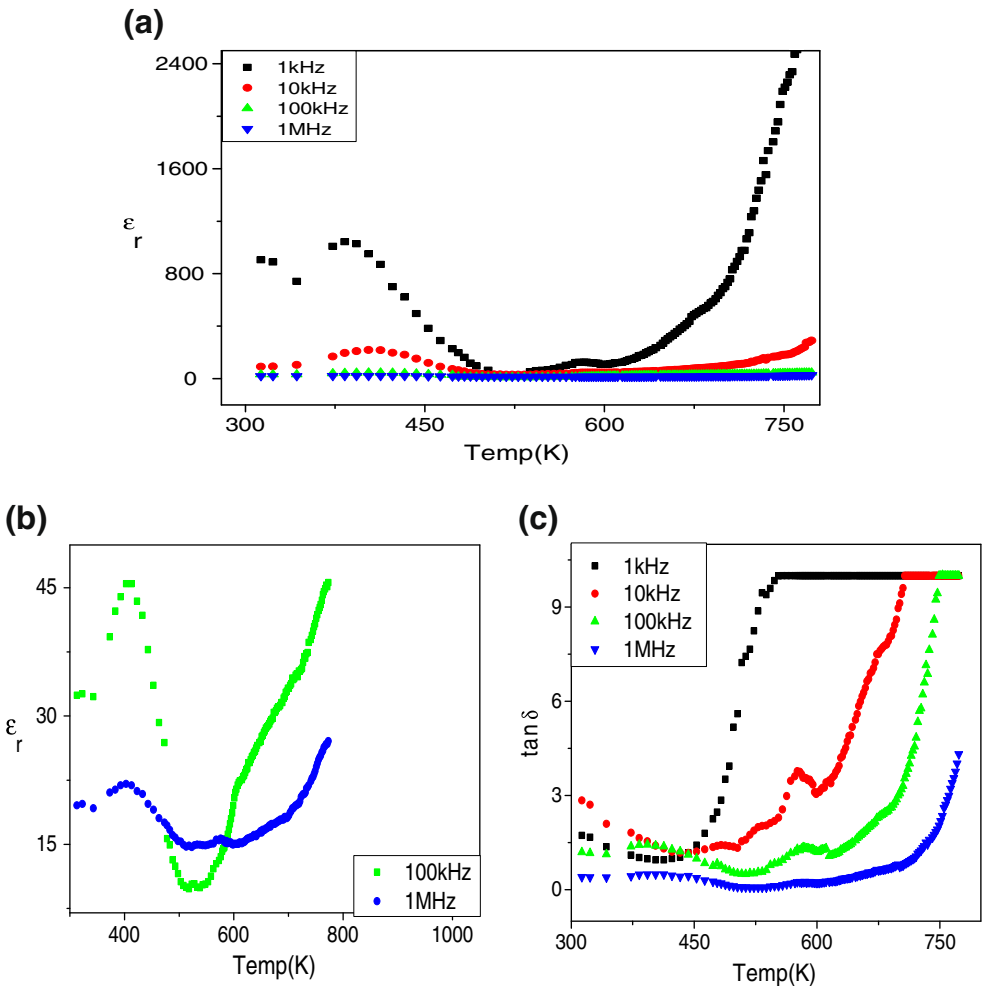

Fig. 3 The temperature dependent (**a**, **b**) dielectric constant (ε_r) and (**c**) loss tangent (tanδ) at 1 kHz, 10 kHz, 100 kHz and 1 MHz of $Ba_5LaTi_3V_7O_{30}$

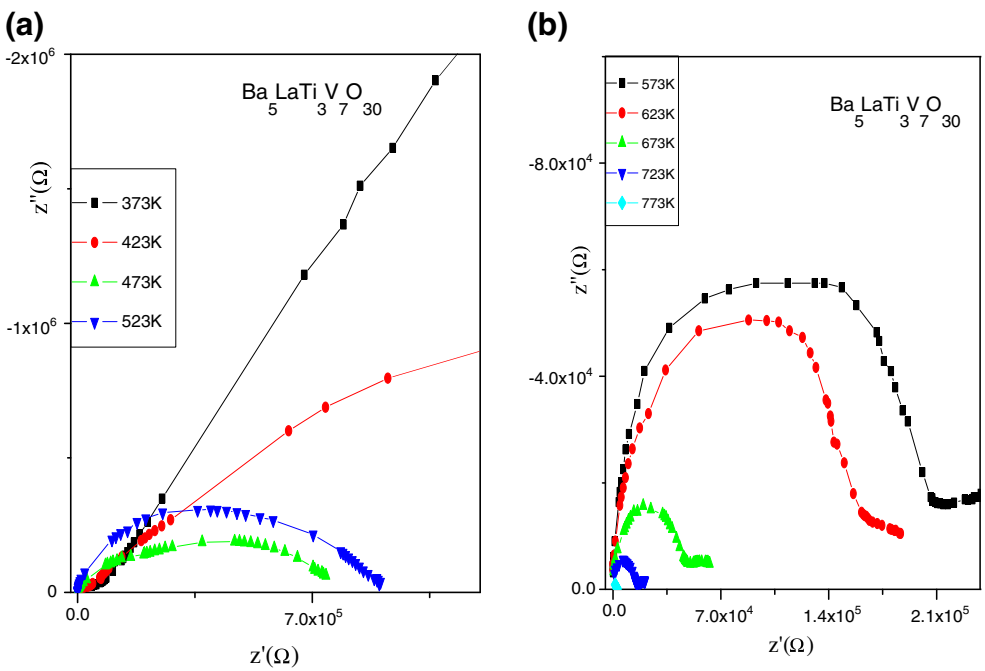

Fig. 4 (**a**, **b**): Impedance plots of $Ba_5LaTi_3V_7O_{30}$ specimen at different temperatures

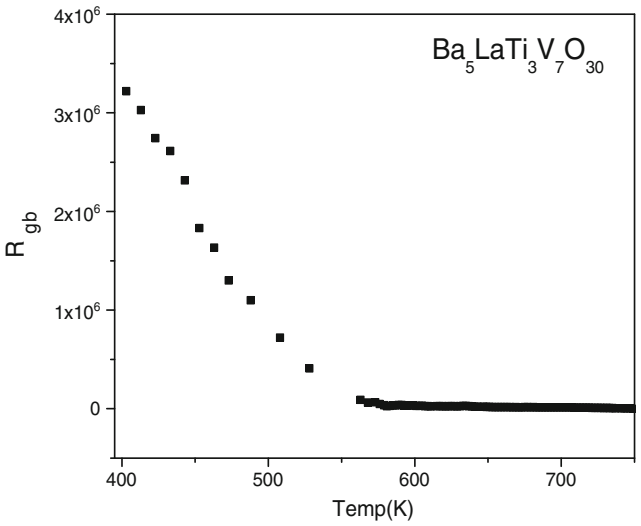

Fig. 5 Variation of R_{gb} with temperature of $Ba_5LaTi_3V_7O_{30}$

The dielectric anomalies at around 413 K, 403 K, 403 K and 403 K for 1 kHz, 10 kHz, 100 kHz and 1 MHz frequencies respectively, were observed in the sample. Dielectric constant at 1 kHz represents the dielectric constant (1043) of grain boundary region and hence its values are very high compared to values at 100 kHz (ε_{max}=45) and 1 MHz (ε_{max}=22) which is due to grain interior effect only. It was found that this compound has a diffused-type dielectric anomaly at T_c indicating the possible occurrence of ferroelectric-paraelectric phase transition. Similar trend in variation of dielectric constant with temperature was observed in the values for all the measured frequencies. The above anomaly is consistent with that observed in earlier article also [16]. The broadening of the dielectric peak may be considered due to heterogeneity in the composition, voids and defects present in the compound and thus a

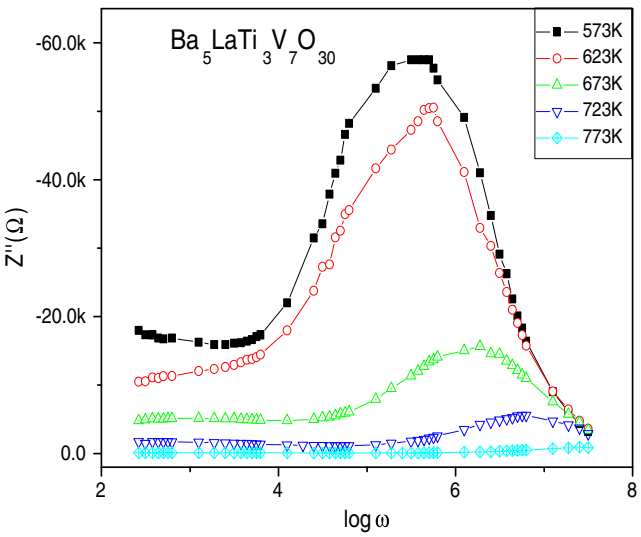

Fig. 6 Temperature dependent Z″ of $Ba_5LaTi_3V_7O_{30}$

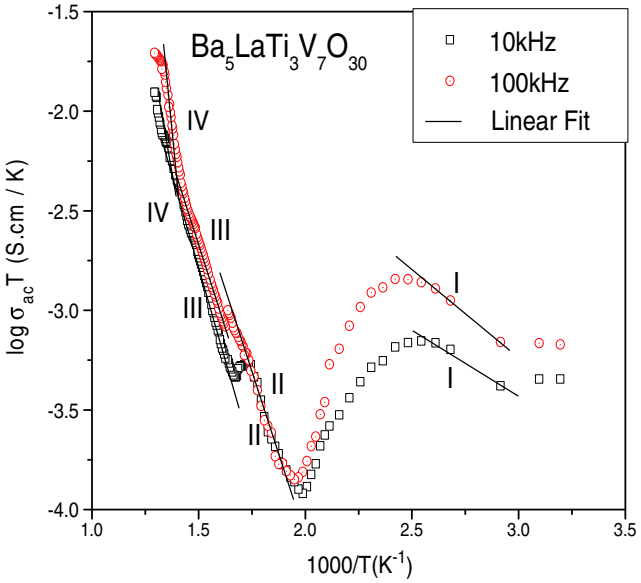

Fig. 7 Variation of log σ_{ac}T with inverse of absolute temperature (10^3/T) of $Ba_5LaTi_3V_7O_{30}$ at different frequencies

distribution of different Curie points results. Similar characteristic has been observed in other members of TB-type structure [18]. Second peak (at around 580 K for 10 kHz) in temperature versus dielectric constant plots is also observed in this compound which could be ascribed to the ionic transition [19] and the value of the dielectric loss is high. Hence, the dielectric constant may have contributions from both dipole orientation and long-range migration of charge species. The higher values of tanδ at high temperatures may be due to the transport of ions with higher thermal energy and is indicative of lossy characteristic of the materials. It is also observed that both ε_r and tanδ decrease with rise in frequency, which is a general feature of polar (ferroelectric) dielectric materials having mobile charge carriers (i.e., ions and electrons) [20]. At low frequency (up to 1 kHz) all types of polarizations (electronic, ionic, dipolar and interfacial polarization) exists. This results in large value of dielectric constant at low frequency. The electronic and ionic polarizations exist up to some mega Hz. At very high frequency, only electronic polarization exists. Hence dielectric constant decreases with frequency. The loss tangent is mostly due to the scattering mechanism

Table 1 Activation energies E_a (eV) from ac conductivity and dc conductivity of $Ba_5LaTi_3V_7O_{30}$ at selected frequencies

f(kHz)	E_a(eV) from ac conductivity			
	Region I	Region II	Region III	Region IV
10	0.13	0.43	0.76	0.71
100	0.15	0.61	0.10	1.41
	E_a(eV) from dc conductivity			
	0.28	1.22	0.83	1.68

of charge carrier or defect. The scattering cross section depends on grain size, inter grain space and grain boundary. Since the powder are pressed into pellet under high pressure and sintered at high temperature, the packing fraction is very high. As a result inter grain space as well as grain boundary is reduced. Hence tanδ decreases at high frequency.

3.4 AC impedance properties

The complex impedance spectroscopy is a method in which the electrical response, in general, is reported in terms of impedance.

Figure 4(a, b) shows the complex impedance spectrum (Z′ vs. Z″) of $Ba_5LaTi_3V_7O_{30}$ at selected temperatures. Two arcs have been observed in a wide temperature range (373 K–773 K). This indicates that the electrical properties of the material arise mainly due to the bulk and grain boundary effects. The display of impedance data in the complex plane i.e., Z′ and Z″ (Nyquist plot) appears in the form of succession of semicircles attributes to relaxation phenomena due to different time constants due to contribution of grain (bulk), grain boundary and interfacial polarization in a material. Hence the contribution to the overall electrical properties by various components is separated out easily. The intercept of first semicircle (in high frequency region) is due to grain (bulk), the second semicircle (at intermediate frequency) is due to grain boundary and the third in low frequency is due to electrode effect. It also indicates that as the temperature increases intercept point on the real axis shifts towards the origin indicating the decrease in the resistivity of the material. This gives the bulk resistance (R_b) of the material. The grain boundary resistance is also evaluated from the impedance spectra and is plotted in Fig. 5. It is also clear from the figure that as the temperature increases grain boundary resistance also decreases their contribution becomes almost temperature independent beyond 700 K.

Figure 6 shows the variation of Z″ with frequency at different temperatures for $Ba_5LaTi_3V_7O_{30}$ compound. It is observed from the plot that (i) the value of Z''_{max} (i.e., peak value) shifts towards higher frequency on increasing temperature (ii) the peak value of Z″ decreases as the temperature increases in the compound (iii) the peaks in the plot could be observed upto a temperature of 723 K. Beyond this temperature peaks could not be observed because it shifts towards higher frequencies which overshoots the limits in which our measurements have been carried out. These observations show the presence of temperature dependent relaxation processes in the systems. The asymmetric peak suggests the existence of a non-Debye type relaxation process in the materials. This non-ideal behavior is co-related to the grain size distribution. The broadening of peaks (explicit plots of Z″) suggests that, there is a spread of relaxation time

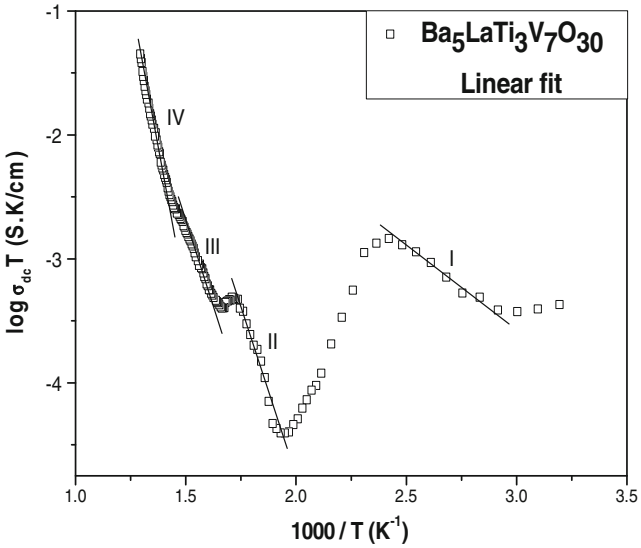

Fig. 8 The bulk dc conductivity in a wide temperature range of $Ba_5LaTi_3V_7O_{30}$

(i.e., the existence of a temperature dependent electrical relaxation phenomenon in the material [21–24]).

3.5 Electrical conductivity study

The ac electrical conductivity (σ_{ac}) was calculated using the dielectric data and an empirical relation [25]; $\sigma_{ac}=\omega\varepsilon_r\varepsilon_o\tan\delta$ where ε_o permittivity in free space, ω angular frequency and tan δ is the dielectric loss, determined by equation tan $\delta=-Z'/Z''$. Figure 7 shows the variation of log $\sigma_{ac}T$ with inverse of absolute temperature (10^3/T) of $Ba_5LaTi_3V_7O_{30}$ at different frequencies. The nature of variation of σ_{ac} over a wide temperature range supports the thermally activated transport properties of the materials obeying Arrhenius equation:

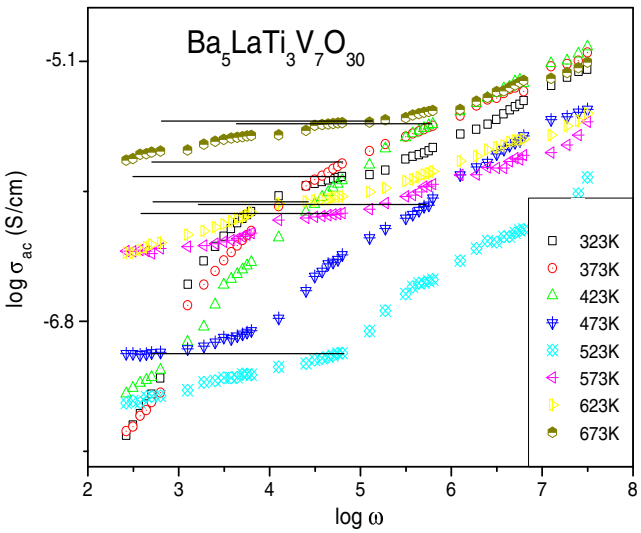

Fig. 9 The frequency dependence of the ac conductivity at different temperatures of $Ba_5LaTi_3V_7O_{30}$

Table 2 Values of σ_{dc} (from impedance plot), σ_{dc} (from σ_{ac} conductivity) and *n* (from Jonscher's universal power law) at selected temperatures for $Ba_5LaTi_3V_7O_{30}$

$Ba_5LaTi_3V_7O_{30}$				
Temp(K)	393	573	623	673
σ_{dc} (from impedance plot)	3.45191e-6	6.97546e-7	9.05388e-7	2.97748e-6
σ_{dc} (from ac conductivity plot)	3.501e-6	7.096e-7	9.311e-7	3.000e-6
n	0.55	0.37	0.24	0.23

$\sigma_{ac}=\sigma_0 \exp(-E_a/K_BT)$, where the symbols have their usual meanings. It is observed that the ac conductivity of the material increases with rise in temperature, and shows the negative coefficient of resistance behavior. The values of E_a (eV) in different regions for ac conductivity and dc conductivity at selected frequencies are summarized in Table 1. The conductivity of the compounds at higher temperature is higher, which is a common behavior of the most of the dielectric ceramics [26, 27]. The nature of variation of σ_{ac} and σ_{dc} over a wide range supports the presence of thermally activated process in the materials. This is due to the presence of immobile species at low temperature, and ions/defects at higher temperatures. From the activation energy, it can be concluded that a small amount of energy is required to activate the charge carriers/electrons for electrical conduction. Similar trend of variation of ac conductivity was observed in some materials of this kind [26]. The bulk dc conductivity (σ_{dc}) [28] of the material was calculated using arcs of complex impedance spectrum (Z′ versus Z″) in a wide temperature range (RT-773 K) as shown in Fig. 8 above. The temperature dependence of dc conductivity (Fig. 8) follows similar nature as followed by the ac conductivity.

In order to further elucidate the transport mechanism in solid solutions, ac conductivity at different frequencies and temperatures was determined by using the dielectric data via equation discussed above. The frequency dependence of the ac conductivity at different temperatures is shown in Fig. 9. At low frequencies, the conductivity shows plateau which corresponds to the dc part of the conductivity. At higher frequencies, the conductivity shows dispersion. It is clear from the figure that the flat region increases with the increase in temperature. In Fig. 9, at all the temperatures, the conductivity is independent of frequency at low frequency regime. The conductivity increases with increasing temperature due to thermal activation of conducting species in the samples.

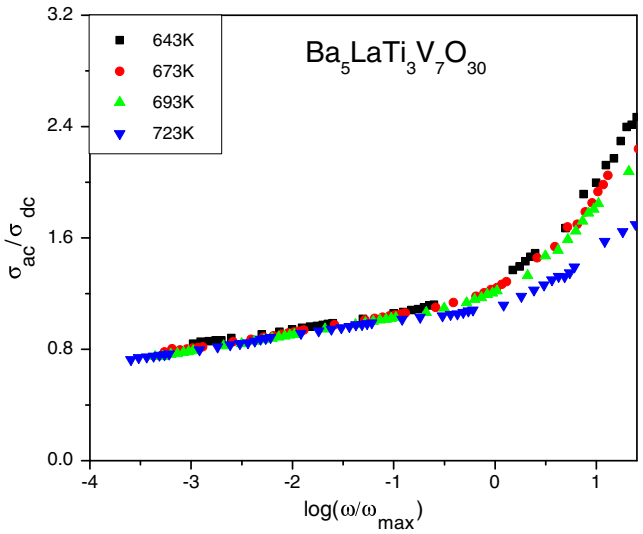

Fig. 10 Log (ω/ω_h) vs σ_{ac} / σ_{dc} at different temperatures for $Ba_5LaTi_3V_7O_{30}$

Figure 9 shows the variation of the ac conductivity (σ_{ac}) as a function of frequency at selected temperatures (i.e., 323 K-673 K). The conductivity is found to be frequency independent in the low frequency region. This result may be due to the short-range hopping between the adjacent sites. The increase in the conductivity with the rise in frequency (high frequency region at different temperatures) is described through Jonscher's universal power law; $\sigma(\omega)=\sigma_{dc}+A\omega^n$ [29] where σ_{dc} is the dc conductivity of the material, A is the dispersion parameter and $0<n<1$ (the dimensionless frequency exponent). Table 2 depicts the values of σ_{dc} (from impedance plot), σ_{dc} (from σ_{ac} conductivity) and *n* (from Jonscher's universal power law) at selected temperatures. σ_{dc} have been evaluated at different temperatures extrapolating the intermediate frequency-independent plateau region of the conductivity plots towards the zero frequency and it is almost same as obtained from impedance plots. In the present study, we found that the values of *n* are 0.55 at 393 K and around 0.3 at 573 K, 623 K, 673 K indicating dominance of ionic transport over electronic at higher temperature. Figure 10 shows $\log(\omega/\omega_h)$ vs σ_{ac}/σ_{dc} plot at different temperatures for $Ba_5LaTi_3V_7O_{30}$, where σ_{ac} is scaled w.r.t σ_{dc} and ω is scaled w.r.t ω_h. From this plot, we obtained a nearly superimposed master curve. Thus the relaxation mechanism found to be temperature independent under conductivity formalism.

4 Conclusion

The $Ba_5LaTi_3V_7O_{30}$ compound of the tungsten-bronze family is ferroelectric and have an orthorhombic crystal structure at room temperature. There is no change in the basic structure of the titled ($Ba_5RTi_3V_7O_{30}$) compound by changing rare earth (i.e by taking the rare earth La). X-ray diffraction analysis confirms the formation of BLTV compounds, having single phase. Microstructural studies reveal that

there is an average grain size of ~3 μm. The dielectric studies show that this compound has a diffused-type dielectric anomaly (i.e., the broad dielectric peaks which is more clearly seen at 1 MHz) at T_c indicating the possible occurrence of ferroelectric-paraelectric phase transition. High value of dielectric loss indicates that dielectric constant may have contributions from both dipole orientation and long range migration of charge species. The complex impedance plots reveal the contribution of grain boundary and bulk effects in it. Negative temperature coefficient of resistance (NTCR) behavior is observed in the compound. The variation of dc conductivity (bulk) as a function of temperature demonstrates that the compound has Arrhenius type of electrical conductivity. The activation energy is found to be 0.15 eV (from ac conductivity at 1 MHz) and 0.28 eV (from dc conductivity) below phase transition. We found that the values of n are 0.55 at 393 K and around 0.3 at 573 K, 623 K, 673 K indicating dominance of ionic transport over electronic at higher temperature.

Acknowledgement Authors thank Director, NERIST to permit to carry out research work and for his encouragement help. We are grateful to the Central Research Facilities of IIT Kharagpur for doing SEM and also thankful to Dr S. R. Shanigrahi (IMRE, Singapore) for his help in XRD, respectively.

References

1. P.B. Jamieson, S.C. Abrahams, J.L. Bernstein, J Chem Phys **50**, 4352 (1969)
2. B.A. Scott, E.A. Geiss, G. Burns, O'Kane, Mat. Res. Bull. **3**(10), 831–842 (1968)
3. N.K. Singh, R.N.P. Choudhary, A. Panigrahi, J Mater Sci Lett **20**, 707 (2001)
4. A. Panigrahi, N.K. Singh, R.N.P. Choudhary, J Mater Sci Lett **18**, 1579 (1999)
5. A. Panigrahi, R.N.P. Choudhary, B.N. Das, Bulletin of Pure and Applied Sci **17**(2), 77 (1998)
6. I. Camlibel, J Appl Phys **4**, 1690 (1969)
7. E.C. Subba Rao, G. Shirane, J Chem Phys **32**, 1846 (1960)
8. E.A. Giess, B.A. Scott, G. Burns, D.F. O'Kane, A. Segmüller, J Am Ceram Soc **52**, 276 (1969)
9. N.K. Singh, A. Panigrahi, R.N.P. Choudhary, Material Letters **50**, 1 (2001)
10. B. Behera, P. Nayak, R.N.P. Choudhary, Material letters **61**, 3859 (2007)
11. M.C. Stennnett, G.C. Miles, J. Sharma, I.M. Reaney, Journal Eur. Ceram. Soc. **25**, 2471 (2005)
12. P.S. Sahoo, A. Panigrahi, S.K. Patri, Central European Journal of Physics **6**(4), 843 (2008)
13. M.R. Ranga Raju, R.N.P. Choudhary, J. Phys. Chem. Solids **64**(5), 847 (2003)
14. A. Panigrahi, N.K. Singh, R.N.P. Chaudhary, Journal of Material Science Letter **18**, 1579–1581 (1999)
15. P.R. Das, R.N.P. Choudhary, J. Phys. Chem. Solids **68**, 516 (2007)
16. K. Kathayat, A. Panigrahi, A. Pandey, S. Kar, Integr Ferroelectr **118**(01), 8–15 (2010)
17. E. Wu,"PowdMult, an interactive powder diffraction data interpretation and indexing program, version 2.5,"Schoolof Physical sciences, Finders University of South Australia, Bedford Park, Australia
18. N.K. Singh, R.N.P. Choudhary, A. Panigrahi, Mater Chem Phys **74**, 116 (2002)
19. M. Dammak, H. Khemakhem, N. Zouari, A.W. Kolsi, T. Mhiri, Solid State Ionics **127**, 125–132 (2000)
20. P.S. Sahoo, A. Panigrahi, S.K. Patri, R.N.P. Choudhary, J Mater Sci Mater Electron **21**, 160–167 (2010)
21. D.C. Sinclair, A.R. West, J Appl Phys **66**, 3850 (1989)
22. K. Srinivas, A.R. James, J Appl Phys **86**, 3885 (1999)
23. D.C. Sinclair, A.R. West, J Mater Sci **29**, 6061 (1994)
24. C.K. Suman, K. Prasad, R.N.P. Choudhary, Adv Appl Ceram **104**, 294 (2005)
25. W.D. Kingery, *Introduction to ceramics* (Oxford University Press, Wiley, New York, 1960)
26. R.N.P. Choudhary, K.S. Singh, R. Sati, Pranama **38**(3), 161 (1992)
27. S. Rao, P.S.V. Rao, K. Sambasiva Rao, A. Bhanumathi, Mater. Sci. Engg. B. **98**(3), 279 (2003)
28. D. Marrero-Lopez, J. Canales-Vazquez, J.C. Rauiz-Morales, A. Rodriguez, J.T.S. Irvine, P. Nunez, Solid State Ionics **176**, 1807–1816 (2005)
29. N. Gogulamurali, S.A. Suthanthiraraj, P. Maruthamuthu, J Mater Sci. **32**, 4175–4179 (1997)